Geophysical Research Letters

RESEARCH LETTER
10.1029/2023GL104847

Deep Convection as the Key to the Transition From Eocene to Modern Antarctic Circumpolar Current

Qianjiang Xing[1], Andreas Klocker[2], David Munday[3], and Joanne Whittaker[1]

[1]Institute for Marine and Antarctic Studies, University of Tasmania, Hobart, Australia, [2]NORCE Norwegian Research Centre, Bjerknes Centre for Climate Research, Bergen, Norway, [3]British Antarctic Survey, Cambridge, UK

Key Points:

- Deep convection is able to drive a strong Antarctic Circumpolar Current (ACC)
- Surface cooling and sea ice formation are crucial drivers of this deep convection
- ACC similar to a rim current around convective sites, energizing ocean circulation

Supporting Information:

Supporting Information may be found in the online version of this article.

Correspondence to:

Q. Xing,
qianjiang.xing@utas.edu.au

Citation:

Xing, Q., Klocker, A., Munday, D., & Whittaker, J. (2023). Deep convection as the key to the transition from Eocene to modern Antarctic Circumpolar Current. *Geophysical Research Letters*, *50*, e2023GL104847. https://doi.org/10.1029/2023GL104847

Received 19 JUN 2023
Accepted 4 DEC 2023

Author Contributions:

Conceptualization: Andreas Klocker, David Munday, Joanne Whittaker
Formal analysis: Qianjiang Xing
Funding acquisition: Andreas Klocker, David Munday, Joanne Whittaker
Investigation: Qianjiang Xing, Andreas Klocker, David Munday, Joanne Whittaker
Methodology: Andreas Klocker, David Munday, Joanne Whittaker
Project Administration: Andreas Klocker, David Munday, Joanne Whittaker
Supervision: Andreas Klocker, David Munday, Joanne Whittaker
Visualization: Qianjiang Xing

Abstract From the Eocene (~50 million years ago) to today, Southern Ocean circulation has evolved from the existence of two ocean gyres to the dominance of the Antarctic Circumpolar Current (ACC). It has generally been thought that the opening of Southern Ocean gateways in the late Eocene, in addition to the alignment of westerly winds with these gateways or the presence of the Antarctic ice sheet, was a sufficient requirement for the transition to an ACC of similar strength to its modern equivalent. Nevertheless, models representing these changes produce a much weaker ACC. Here we show, using an eddying ocean model, that the missing ingredient in the transition to a modern ACC is deep convection around the Antarctic continent. This deep convection is caused by cold temperatures and high salinities due to sea-ice production around the Antarctic continent, leading to both the formation of Antarctic Bottom Water and a modern-strength ACC.

Plain Language Summary The evolution of ocean circulation from the early Southern Ocean around 50 million years ago to today has seen much debate over the past decades. The main characteristic of the modern Southern Ocean is the prevalence of the Antarctic Circumpolar Current (ACC), the world's strongest current. In the past it has been thought that the deepening of ocean gateways, and changes in the strength and location of winds, led to an ACC of similar strength to its modern equivalent. Nevertheless, ocean models simulating these changes typically reproduce an ACC with less than a third of the modern ACC's strength. Here we show that the missing ingredient in the transition to a modern ACC is deep convection around the Antarctic continent. Deep convection is due to a combination of cooling and increase in salinity by sea ice formation which allows for water at the ocean surface to become denser than the water below, leading to the mixing of the water column to great depths. This deep convection allows for the ocean to be energized, leading to a modern-strength Antarctic Circumpolar Current. A cool climate around the Antarctic continent is therefore crucial for the development of a modern-strength Antarctic Circumpolar Current.

1. Introduction

In recent decades, proxy techniques and model experiments have been applied to explore the evolution of Southern Ocean circulation from the late Eocene pattern of two gyres (the subtropical and subpolar gyres) to the modern Antarctic Circumpolar Current (ACC) (D. J. Hill et al., 2013; Sauermilch et al., 2021; Scher et al., 2015; Sijp & England, 2004; Stickley et al., 2004). The modern ACC is characterized by a circumpolar pathway penetrating both Tasman Gateway (TG) and Drake Passage (DP), with a volume transport through the DP of 137 Sv (Meredith et al., 2011, 1 Sv = 10^6 m^3s^{-1}), or around 173 Sv if the near-bottom flow is included (Donohue et al., 2016). There are several common factors that might have played a role in the development of the modern ACC—the opening and deepening of ocean gateways, changes in the wind forcing, and changes in buoyancy forcing. In previous studies, the opening and the deepening of ocean gateways (Baatsen et al., 2020; D. J. Hill et al., 2013; Sijp et al., 2011), the change in strength and location of wind stress (Sauermilch et al., 2021; Scher et al., 2015; Xing et al., 2022), and the declining of atmospheric CO_2 (Goldner et al., 2014; Ladant et al., 2014; Lefebvre et al., 2012) have been shown to have critical roles in the development of the proto-ACC and the transition of the early Southern Ocean toward its modern circulation. Nevertheless, all the studies obtain a DP transport of the proto-ACC not exceeding 90 Sv, even with a deep TG (1,500 m; DP transport of 12.5 Sv) (Sauermilch et al., 2021) and/or strong wind stress (maximum wind stress of 0.2 N m^{-2}; DP transport of 44.8 Sv) (Xing et al., 2022), or modern pCO_2 (280 ppm; DP transport of 89 Sv) (Lefebvre et al., 2012). Hence, these so-called proto-ACCs are quite different from the realistic modern ACC regarding DP transport. This raises the question of what drives the increase of the ACC's transport through DP toward its modern value.

Writing – original draft: Qianjiang Xing
Writing – review & editing: Andreas Klocker, David Munday, Joanne Whittaker

In the traditional paradigm, the Southern Ocean's strong westerly surface winds are considered to be a prominent driver of the ACC (Allison et al., 2010; Gnanadesikan, 1999), although surface buoyancy forcing has been recognised as of importance (Hogg, 2010). The westerly winds drive a northward Ekman transport, which acts to steepen isopycnal surfaces across the Southern Ocean (J. Marshall & Radko, 2003). This produces a meridional gradient in density, which varies with depth, and consequently leads to an eastward ACC via thermal wind shear (Vallis, 2017). Despite this focus on surface wind stress as a driver of the ACC, eddying model simulations show that its circumpolar volume transport is insensitive to changes in wind forcing (Hallberg & Gnanadesikan, 2001; Tansley & Marshall, 2001), potentially to the limit of no wind (D. R. Munday et al., 2013, 2015). This contrasts to the response of models that must parameterize eddies due to their resolution (McDermott, 1996; Toggweiler & Samuels, 1995, 1998). Note that recent parameterizations that keep track of eddy energy are able to partially replicate this behavior (Mak et al., 2018).

Based on experiments with turbulence-resolving direct numerical simulations (Barkan et al., 2013; Gayen & Griffiths, 2022; Klocker et al., 2023; Sohail et al., 2019; Xing et al., 2023), it has been suggested that rotating horizontal convection may play a role in the ACC's formation. Rotating horizontal convection is driven by surface buoyancy loss and gain (Gayen & Griffiths, 2022; Hughes & Griffiths, 2008) with deep convection taking place at the boundary where buoyancy is lost. This ties the formation of the ACC to the presence of such convection and thus the formation of deep and bottom waters. In a simple reduced gravity model of the ACC, the initiation of deep water formation leads to the acceleration of the ACC and a large increase in its circumpolar zonal transport (D. R. Munday et al., 2022). In addition, two model studies propose that the presence of ice sheets and brine rejection from sea-ice formation can lead to acceleration of the ACC via thermal wind shear (Ladant et al., 2014; Lefebvre et al., 2012).

The modeling studies discussed above mostly use varying degrees of idealization, whether in domain geometry or in the equations that govern the evolution of the circulation. Lefebvre et al. (2012) and Ladant et al. (2014) both use a realistic geometry, but coarse resolution models in which eddies are parameterized. Our motivation in this study is therefore to test these ideas in an eddying model simulation using a realistic late Eocene bathymetry to see if the change from Eocene to modern surface buoyancy forcing can explain the evolution of the ACC from its weak state in the late Eocene to its modern state with a transport similar to that observed in observations.

2. Methods

The ocean model configuration used in this study is based on an ocean-only configuration of the MIT general circulation model (J. Marshall, Adcroft, et al., 1997; J. Marshall, Hill, et al., 1997), and is identical to that used by Sauermilch et al. (2021) and Xing et al. (2022). The model has 1/4° horizontal grid spacing (i.e., mesoscale eddy-permitting), 50 unevenly spaced vertical levels, and a circumpolar domain with latitude range between 84°S and 25°S. A 300 km sponge layer is used at the northern boundary of the model, restoring the temperature and salinity to a fixed vertical profile with a timescale of 10 days. These temperature and salinity profiles are temporal and zonal mean values taken from a coupled atmosphere–ocean model representing the late Eocene (Hutchinson et al., 2018), and are shown in Figure S1 in Supporting Information S1. Using such boundary conditions assumes that processes in the northern hemisphere, such as deepwater formation in the North Atlantic, are constant for all experiments. This setup therefore allows us to focus entirely on the dynamics in the Southern Ocean. We also apply zero meridional velocities at the northern boundary to maintain volume conservation in our model domain.

Antarctic ice sheet and sea-ice formation are excluded in our model configuration due to computational expense and complexity. However, their impacts in accelerating the ACC will be implicitly felt in our simulations due to using the modern surface buoyancy forcing. The model domain, late Eocene bathymetry, and applied zonally averaged paleo-wind stress are shown in Figure 1. We refer to Sauermilch et al. (2021) and Xing et al. (2022) for more details about this model configuration and paleo-bathymetric reconstruction.

This study uses four sets of surface buoyancy forcing, created following the three steps below, to test its role in the sensitivity of the proto-ACC:

- The late Eocene surface buoyancy forcing (*paleo_SBF*) is derived from sea surface temperature (SST) and salinity (SSS) distributions of a coupled late Eocene (38 Ma) atmosphere–ocean model (Hutchinson et al., 2018), shown in Figures 1b and 1c.

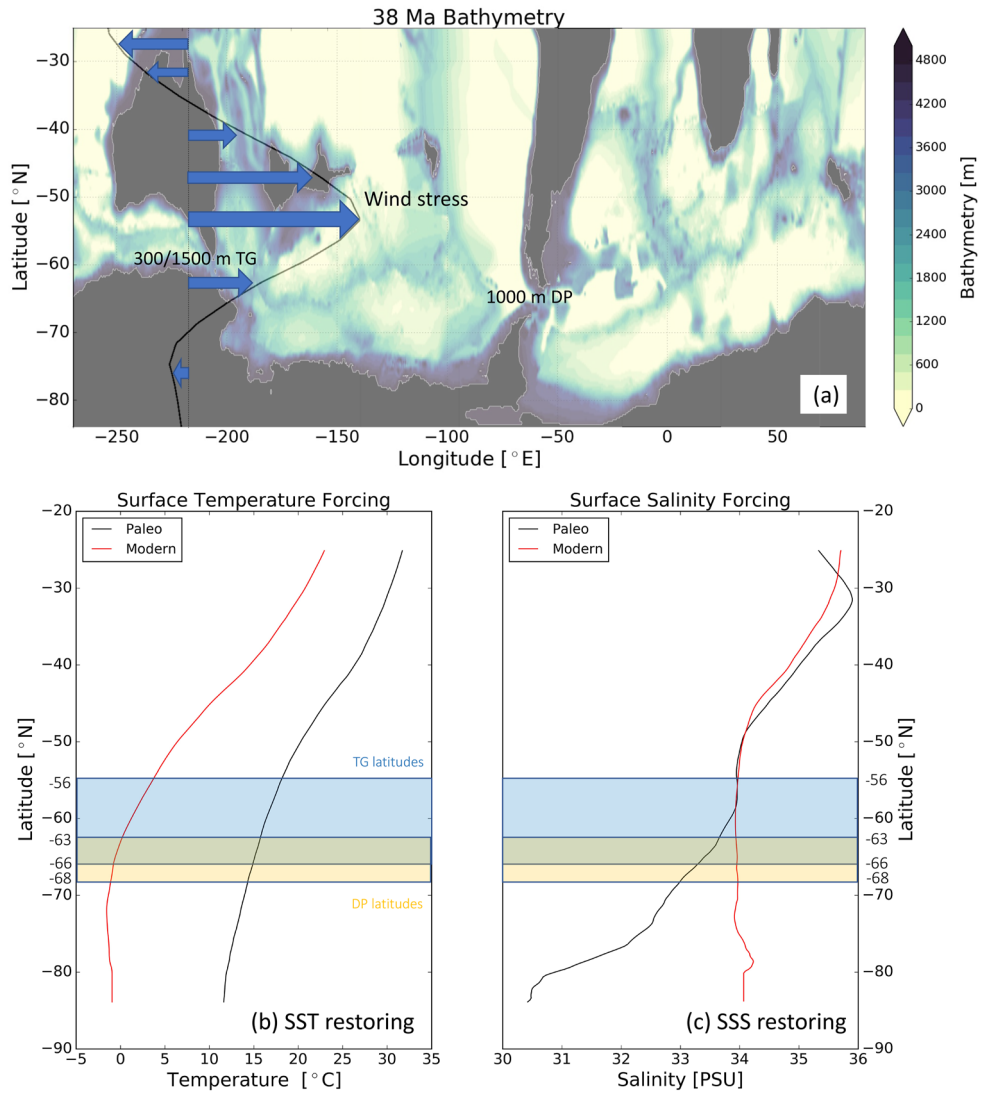

Figure 1. (a) High-resolution (0.25°) reconstructed bathymetry of the late Eocene (38 Ma) Southern Ocean. The black curve and blue arrows show the applied zonal mean wind stress throughout the domain. Peak westerly wind is at about 53°S and has a strength of around 0.1 N m^{-2}. (b, c) Comparisons of late Eocene (black) and modern (red) sea surface temperature restoring (b) and sea surface salinity restoring (c). Blue and yellow rectangles in panel b and panel c indicate the latitude range of the TG and DP.

- The modern surface buoyancy forcing (*modern_SBF*) is derived from SST and SSS distributions of Monthly Isopycnal and Mixed-layer Ocean Climatology (MIMOC) (Johnson et al., 2012). MIMOC records three-dimensional global monthly ocean property distributions within 80°S to 90°N at 0.5° lateral grid spacing. Note that MIMOC only covers the domain with a southernmost latitude of 80°S. To match the applied ocean model domain, we extend eight grid boxes to 84°S using the southernmost data points.
- Based on late Eocene and modern surface buoyancy forcing, we derive another two paleo-modern mixed buoyancy forcing (*paleo_T_modern_S* and *modern_T_paleo_S*). The mixed forcing, for example, *modern_T_paleo_S,* is composed of one modern forcing, for example, modern SST, and one late Eocene forcing, for example, paleo SSS.

We interpolate all surface buoyancy forcing on to the 1/4° grid. Temporal and zonal means of the sea surface temperatures (SST) and salinities (SSS) of these four forcing sets (shown in Figure 1) are then used to restore surface ocean values with a time scale of 10 days. Only the first forcing set, *paleo_SBF,* is fully consistent with the forcing at the northern boundary.

Table 1
Overview of Sensitivity Experiments

Experiments	TG depths (m)	Temperature/Salt forcing	DP transport (Sv)	EKE ($m^4\ s^{-2}$)
300_paleo_SBF	300	Paleo/Paleo	2.8	$3.3*10^{11}$
300_Modern_SBF	300	Modern/Modern	−0.5	$35.4*10^{11}$
1500_paleo_SBF	1500	Paleo/Paleo	13.8	$3.5*10^{11}$
1500_paleo_T_modern_S	1500	Paleo/Modern	17.4	$6.1*10^{11}$
1500_modern_T_paleo_S	1500	Modern/Paleo	70.3	$31.4*10^{11}$
1500_modern_SBF	1500	Modern/Modern	139.2	$42.5*10^{11}$

Note. The column "Experiments" gives names for each case. The columns "Temperature/Salt forcing" show the applied surface buoyancy forcing (Paleo or Modern) for each case. For example, 1500_modern_T_paleo_S indicates the experiment with 1,500 m TG, modern surface temperature forcing, and late Eocene (paleo) surface salt forcing. The column "DP transport (Sv)" and "EKE ($m^4\ s^{-2}$)" give the ACC transport through the DP and horizontal integrated surface eddy kinetic energy, respectively. Note that the DP depth is set to a constant of 1,000 m for all experiments.

As shown in Figure 1, modern SST has a similar meridional gradient to the late Eocene SST, but absolute values are around 10°C colder with freezing temperatures close to the Antarctic coast. Late Eocene and modern SSS have similar values to the north of 60°S, but south of 60°S modern SSS remains around 34 PSU due to sea ice formation, while late Eocene SSS in this area is fresh due to runoff from the continent. The applied modern surface buoyancy forcing (*modern_SBF*) shows low temperatures and high salinities typical of modern high latitudes, which will give a higher density than the Eocene forcing, leading to destabilizing surface buoyancy forcing and hence convection.

In total six experiments are considered, as shown in detail in Table 1. The two model simulations of Xing et al. (2022) with 300 and 1,500 m TG (DP depth: 1,000 m) and late Eocene surface buoyancy forcing have been run for 145 model years to reach equilibrium (*300_paleo_SBF* and *1500_paleo_SBF*). Based on these two control experiments, we conduct four sensitivity experiments (*300_modern_SBF, 1500_paleo_T_modern_S, 1500_modern_T_paleo_S,* and *1500_modern_SBF*) where we apply a mixture of late Eocene and modern surface buoyancy forcing, that is, *modern_T_paleo_S,* or a pure modern surface buoyancy forcing (*modern_SBF*) (see details in Table 1). All sensitivity simulations are run for 145 model years to reach equilibrium (see Figure S2 in Supporting Information S1) and the final 15 years are used to analyze results.

Note that, despite the use of a realistic paleobathymetry, the simulations shown here are semi-idealized. One the one hand, the northern boundary condition acts to keep all processes north of the domain, such as the formation of North Atlantic deep water, constant, allowing us to focus on the role of convection around Antarctica. On the other hand, this domain can therefore not simulate the interaction between deepwater formation in the south and in the north. This domain also allows a spinup of eddying, and hence computationally expensive, simulations which would be over an order of magnitude more expensive if the domain were global. The representation of eddies is crucial since the ACC strength is a balance between processes that steepen isopycnals, for example, convection or wind stress, and eddies flattening them (Johnson & Bryden, 1989; D. Marshall, 1997; J. Marshall & Radko, 2003; Klocker et al., 2023). Parameterized eddies might therefore produce misleading results. These idealized experiments therefore allow for simulations in which eddies are partially resolved, which has been shown to be crucial to correctly simulate ACC dynamics (Hallberg & Gnanadesikan, 2001, 2006; D. R. Munday et al., 2013; Straub, 1993; Tansley & Marshall, 2001), and allow to isolate the effect of convection along the Antarctic coast, but come with the caveat that changes in the Southern Ocean cannot interact with the dynamics in the northern hemisphere. Given these pros and cons, the results of our simulations should be seen as complementary to previous work using coarse-resolution simulations of a global coupled ocean-atmosphere system, such as those by Ladant et al. (2014) and Lefebvre et al. (2012).

3. Results

3.1. Changes in Temperature, Salinity, and Zonal Velocity

We show meridional sections of temperature, salinity, and zonal velocity across the central Pacific (150°W) for the three experiments *300_paleo_SBF* (Figure 2 Row A1-3), *1500_paleo_SBF* (Figure 2 Row C1-3), and

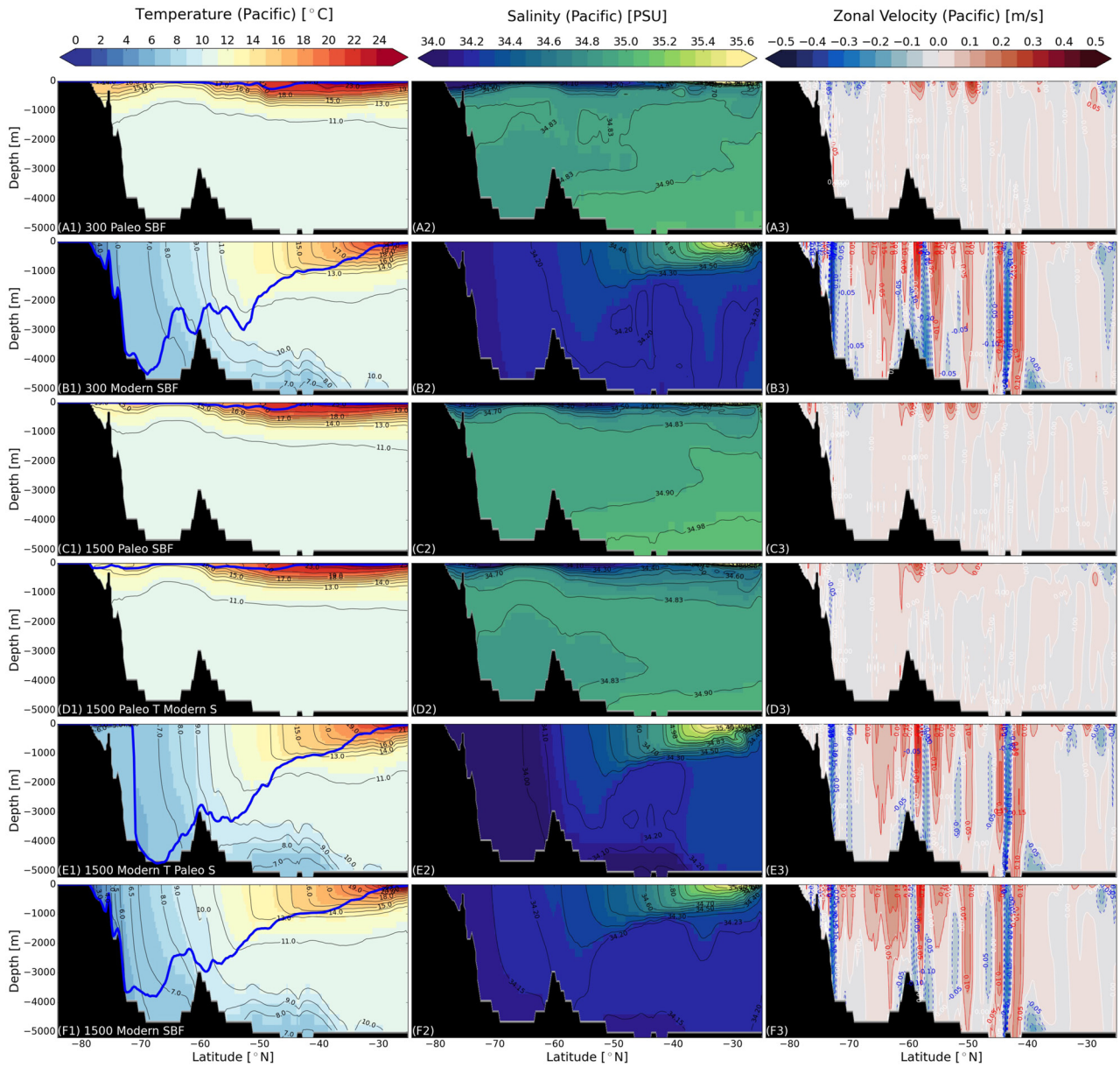

Figure 2. Pacific meridional sections (150°W) of temperature (Column 1), salinity (Column 2), and zonal velocity (Column 3) for *300_paleo_SBF* (Row A1-3), *300_modern_SBF* (Row B1-3),*1500_paleo_SBF* (Row C1-3), *1500_paleo_T_modern_S* (Row D1-3), *1500_modern_T_paleo_S* (Row E1-3), and *1500_modern_SBF* (Row F1-3). Blue curves in panels of Column 1 indicate mixed layer depth at 150°W.

1500_paleo_T_modern_S (Figure 2 Row D1-3). We find that these experiments show bowl-shaped isotherms and isohalines in the latitudes of 70°S to 60°S and 45°S to 30°S, associated with subpolar and subtropical gyres in the upper ocean. These concentrated isotherms and isohalines in the upper ocean show strong near-surface stratification, restricting vertical movement of surface water. The westward (blue) and eastward (red) jets, also confined to the upper ocean, indicate the location and boundaries of subpolar and subtropical gyres. These jets are due to thermal wind concentrating vertical shear into the top ~1,000 m.

In experiments *300_modern_SBF* (Figures 2B1 and B2), *1500_modern_T_paleo_S* (Figures 2E1 and E2), and *1500_modern_SBF* (Figures 2F1 and F2), the hydrographic distributions of temperature and salinity show strong meridional gradients from 25°S to 80°S. High temperature and salinity occur in the upper ocean from 25°S to 55°S. These are similar to observations of the modern Southern Ocean (Talley, 1996). However, these simulations typically all show a full-depth column of fresher water (about 34 PSU) at high latitudes relative to low

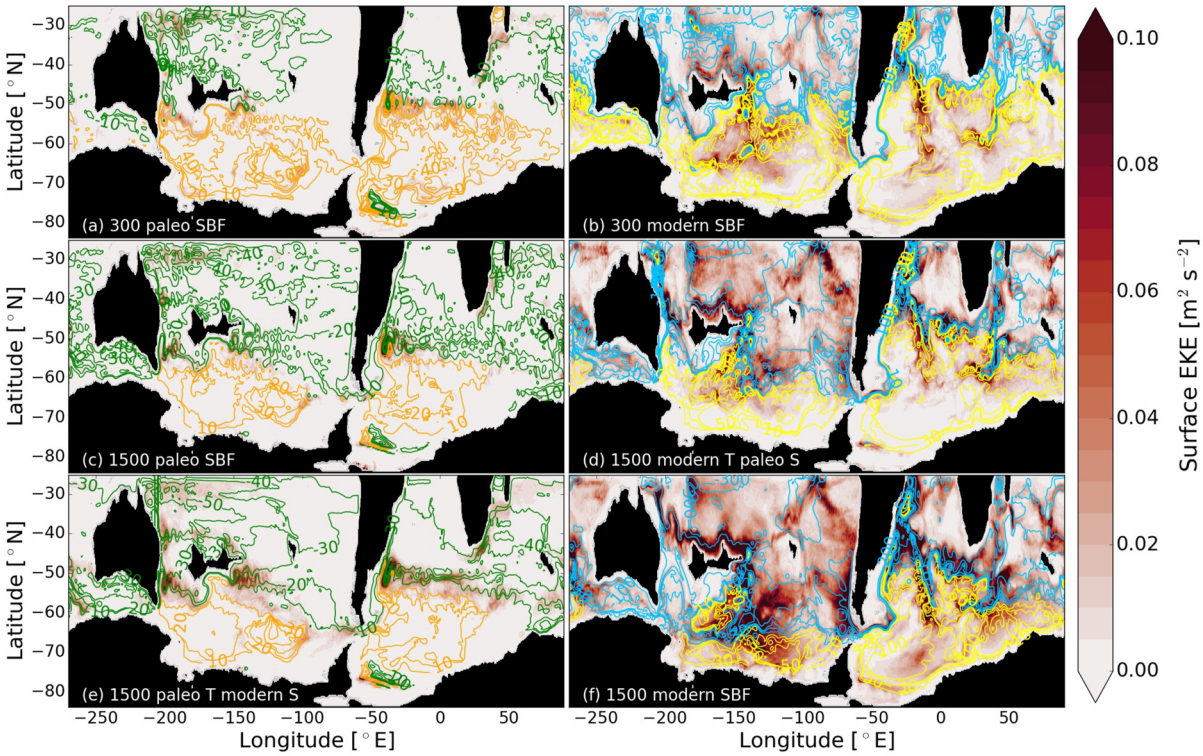

Figure 3. Spatial distribution of ocean surface eddy kinetic energy (EKE) [$m^2\ s^{-2}$]. Green (ranges between −50 and 0 Sv) and blue (ranges between −300 and 0 Sv) contours show depth-integrated stream function of subtropical gyres, orange (ranges between 0 and 50 Sv) and yellow (ranges between 0 and 300 Sv) contours indicate depth-integrated stream function of subpolar gyres.

latitudes, which is inconsistent with observations that show such fresher water only confined to the surface. This could be due to either the absence of seasonal surface forcing, or the absence of North Atlantic Deep Water moving toward the southern high latitudes. Despite the differences of these simulations compared to the modern ocean, which we do not try to exactly reproduce in our idealized simulations, these simulations show the typical steep isopycnals across the Southern Ocean, associated with a strong ACC.

All three experiments show extremely steep isotherms and isohalines in the latitudes of 70°S to 40°S, those south of 60°S even extend to the ocean floor, indicating full-depth weak stratification accompanied by deep convection, as shown by the deep mixed layers south of 60°S (blue curves in Figure 2 and details in Section 3.2). These mixed layers will cause temperature and salinity to be strongly mixed in the vertical. As a result of the steep isopycnals, the zonal velocities south of 40°S become much stronger and reach the bottom in all three experiments. These deep-reaching velocities are associated with a strong thermal-wind driven current, which is baroclinically unstable and able to generate energetic eddy fields, shown in Figure 3. Note that the polar region (south of 70°S) of the experiment *1500_modern_T_paleo_S* sustains high stratification of the polar water in the shallow ocean due to the low local SSS restoring (around 31–33 [PSU]).

3.2. Deep Convection Energizes Southern Ocean Circulation

To investigate the dynamics driving changes in simulated Southern Ocean properties, we show the mixed layer depth (Figure 2, blue curves in the left column), surface eddy kinetic energy (EKE) (Figure 3, red color and Table 1) and depth-integrated stream function (Figure 3, contours). From Figure 2, we can see that experiments *300_paleo_SBF* (Figure 2A1), *1500_paleo_SBF* (Figure 2C1), and *1500_paleo_T_modern_S* (Figure 2D1) lead to shallow mixed layer depth in the latitudes of 40°S to 60°S. These shallow mixed layers are consistent with strong stratification in the upper ocean. These three experiments also share a similar distribution of low eddy activity (Figures 3a, 3c, and 3e) with the exception of regions with enhanced EKE that occur along the boundary between the subtropical and subpolar gyres. These low EKE fields are consistent with the locally flat isotherms,

isohalines, and weak zonal velocities (Figure 2Row A,C,D). The subtropical and subpolar gyres in these experiments have strengths of around −50 to 50 Sv.

In contrast, in experiments *300_modern_SBF* (Figure 2B1), *1500_modern_T_paleo_S* (Figure 2E1), and *1500_modern_SBF* (Figure 2F1), mixed layer depths in most areas of the Southern Ocean are deeper than 1000 m. Those in the latitudes south of 60°S even reach the ocean floor (about 4,500 m). The full-depth mixed layers imply vigorous deep convection occurring in these regions, which are closely associated with the extremely weak stratification and deep-reaching zonal jets (Figure 2). For experiment *1500_modern_T_paleo_S,* the mixed layer is very shallow south of 70°S (Figure 2E1) due to much lower late Eocene salinity near Antarctica. This is associated with low EKE in the same regions.

Two experiments, *1500_modern_T_paleo_S* and *1500_modern_SBF,* using deep TG and modern SST, show similar high EKE fields along the eastern coast of Australia, the northern and eastern coast of New Zealand, the northern part of Drake Passage, the eastern coast of South America, and Agulhas region (see Figures 3d and 3f). The large overlap between high EKE field, deep mixed layers (Figure S1 in Supporting Information S1), and steep isotherms and isohalines (Figure 2) in both experiments implies that the full-depth deep convection homogenizes the water column and raises its center of mass, which leads to steep isopycnals. Baroclinic instability draws on the increased available potential energy and releases it in the form of EKE (Gayen & Griffiths, 2022). These simulated high EKE regions emerge in different areas, but are of similar strength, to observations of the modern Southern Ocean (Le Traon et al., 1998) and model simulations (Bernard et al., 2006; Delworth et al., 2012; Kiss et al., 2020; D. R. Munday et al., 2021). In addition, Figure 3 shows a high positional consistency between high EKE regions and streamlines of gyres boundary, with the subtropical and subpolar gyre enhanced to around −300 to 300 Sv.

These experiments show consistently that deep convection energizes ocean circulation, with the horizontally integrated eddy kinetic energy (EKE) in all experiments with deep convection being approximately an order of magnitude larger than in the experiments without deep convection (Table 1). Deep convection therefore facilitates the conversion of potential energy, supplied by surface buoyancy forcing, into kinetic energy, as seen in the strength of the ACC and gyres, and the increase in EKE.

3.3. Changes in Proto-ACC: Strengthened Transport

The net zonal volume transports of the proto-ACC through both TG and DP, with shallow (300 m) and deep (1,500 m) TG and late Eocene surface buoyancy forcing have been calculated in Xing et al. (2022). With a 300 m TG, a 2.8 Sv net eastward (positive) transport is allowed for both TG and DP throughflow (*300_paleo_SBF*). Using modern surface buoyancy forcing instead (*300_modern_SBF*) results in an increase in eastward TG transport to 25.3 Sv, with a weak westward (negative) DP transport of 0.5 Sv. The weak DP transport is likely due to the compensation between enhanced subtropical and subpolar gyres across the DP (see streamfunction in Figure 3b). With a 1,500 m TG, Xing et al. (2022) has simulated 29.3 and 13.8 Sv for TG and DP transport with late Eocene bathymetry, wind stress, and surface buoyancy forcing (1500_paleo_SBF). The perturbation experiment in this study, using modern SSS and paleo SST, only strengthens TG and DP transport to 30.9 and 17.4 Sv, respectively (*1500_paleo_T_modern_S*). All these weak transports, except ones in experiment *300_modern_SBF,* are associated with strong stratification in the surface ocean and shallow mixed layer depth.

A sharp enhancement in proto-ACC transport relative to *1500_paleo_SBF* occurs when using modern SST and paleo SSS (*1500_modern_T_paleo_S*) as TG and DP transport are intensified to 140.3 and 70.3 Sv, respectively. These enhanced transports are associated with weak stratification and deep convection in high southern latitudes. However, the DP transport is only strengthened to around half of modern ACC value, probably due to low surface salinity around Antarctica restricting local vertical convection. In *1500_modern_SBF,* the simulated proto-ACC is further strengthened, with TG and DP transport of 223.1 and 139.2 Sv, respectively. These values are consistent with observations and model estimates of TG transport (147 Sv (Rintoul et al., 2001) and 164 Sv (Mazloff et al., 2010)); and of DP transport (137 Sv (Meredith et al., 2011) and 155 Sv (Meijers et al., 2012)) (Figure 4). The DP transport is also estimated around 173 Sv when the near bottom flow is included (Donohue et al., 2016). Combining the weak stratification and full-depth mixed layer (Figures 2F1 and F2) in the mid-high latitudes of this experiment, the modern-type ACC can be obtained under the condition of a deep TG and deep convection triggered by modern surface buoyancy forcing, at least in terms of consistent gateway transports.

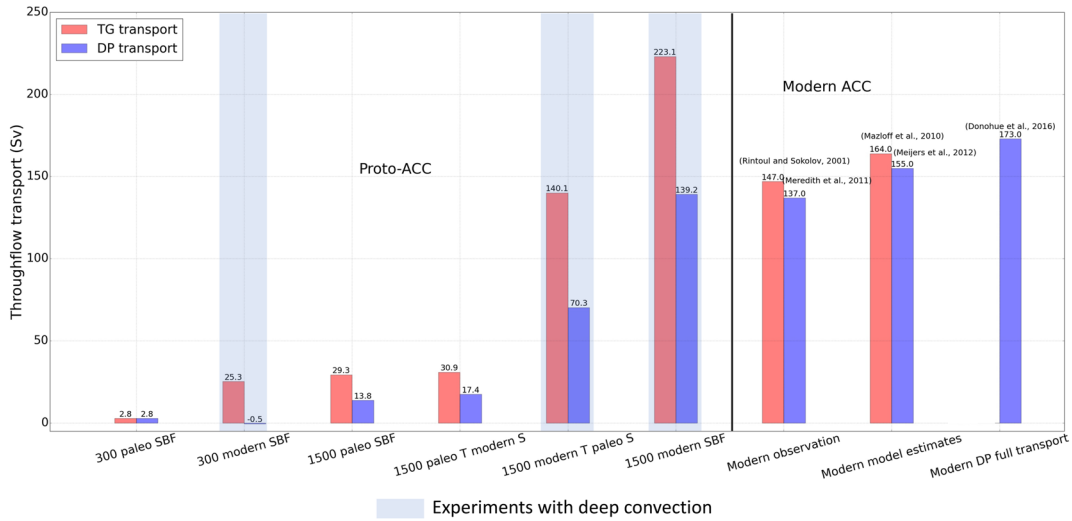

Figure 4. Net TG (red) and DP (blue) transport (Sv). Positive values indicate eastward transport, and negative values indicate westward transport. Left of the black vertical line: Modeled mean transports from this study. Right of the black vertical line: Observed transports from (Meredith et al., 2011; Rintoul & Sokolov, 2001), and modeled transport for the modern ACC from Mazloff et al. (2010) and Meijers et al. (2012). The modern observed DP transport including near bottom flow is 173 Sv (Donohue et al., 2016). Experiments with blue shading means that there is deep convection in the Southern Ocean.

4. Discussion and Conclusions

It has previously been proposed that the deepening of the Tasman Gateway (TG), and the alignment of the westerly winds with the TG, are vital prerequisites for the inception of a proto-ACC during the Eocene-Oligocene Transition (EOT) and its evolution to a modern-strength ACC (Sauermilch et al., 2021; Scher et al., 2015; Sijp et al., 2011; Xing et al., 2022). Nevertheless, model simulations taking into account these changes in bathymetry and winds do not produce an ACC with a transport comparable to its modern values (D. J. Hill et al., 2013; Sauermilch et al., 2021; Xing et al., 2022). Building on recent work which shows that a strong ACC can be generated by convection adjacent to the Antarctic continent (Klocker et al., 2023), we now test if convection could act as the main source of energy accelerating the ACC from its inception at the EOT to its modern strength. To this end, we use an eddying ocean model with realistic late Eocene bathymetry to run multiple simulations with surface buoyancy forcing that either allows or does not allow for convection to occur. These simulations include both a shallow (e.g., 300 m) and a deep (e.g., 1,500 m) TG, to test the effect of these changes on ACC transport.

If the TG remains shallow, changing from paleo temperature and salinity surface forcing to its modern equivalent leads to the appearance of deep convection around the Antarctic continent. The appearance of convection increases the eddy kinetic energy (EKE) in the domain by almost an order of magnitude. This shows how convection acts as a process which allows for the conversion of potential energy, supplied by the surface buoyancy forcing, to kinetic energy in the ocean. Despite this increase in EKE, the ACC transport for this simulation is close to zero, showing that deep convection itself is not sufficient to generate a modern-strength ACC. With a deep TG, the same change from paleo to modern surface forcing also allows for deep convection to occur, including an increase in EKE by about an order of magnitude. However, in the case of a deep gateway, the proto-ACC transport now increases to approximately match its modern value. In summary, for all bathymetric configurations, convection caused by destabilizing surface buoyancy forcing leads to a more baroclinically unstable ocean. This allows for the potential energy supplied by surface buoyancy forcing to be converted to kinetic energy. If, in addition, ocean gateways are deep, convection also leads to a strong ACC, with dynamics similar to rim currents observed around open-ocean deep convection (Send & Marshall, 1995).

The simulations with modern and paleo surface forcing, and combinations of modern/paleo temperature/salinity, seem to suggest that the temperature forcing has a much stronger impact on triggering convection than salinity. This result would, at first sight, argue against the role of increased sea-ice formation in generating convection and hence a strong ACC. This apparent contradiction is likely due to nonlinearities in the equation of state of seawater. These nonlinearities lead to a situation where in a warm ocean, such as the Eocene or the modern tropical and

mid-latitude ocean, temperature has a dominant role in setting density. In contrast, in a cold ocean, such as the modern polar oceans, salinity is dominant in setting density (Roquet et al., 2022). That is, the colder the ocean gets, the more salinity becomes dominant in setting density, in particular in polar latitudes. These thermodynamic effects could have played an important role in the evolution between past warm and cold climates, but have seen little research efforts aimed at understanding these thermodynamic effects.

Our results are consistent with studies by Lefebvre et al. (2012) and Ladant et al. (2014), which both use a coarse-resolution ocean-atmosphere model to show the important role of cooling around the Antarctic continent, and the subsequent sea ice formation, for generating a strong ACC. The main difference to these previous studies is that in our study ocean eddies are partially resolved, whereas previously they were parameterized. Partially resolving eddies allows us to understand changes in eddy kinetic energy in the presence of convection, and to model a more realistic ACC transport. Despite these differences, all these studies, including ours, help to build up solid evidence for the crucial role of deep convection around the Antarctic continent in generating a strong ACC. This shows that the ACC can be a consequence of Antarctic cooling, rather than the Antarctic cooling being a consequence of a thermal barrier created by the ACC. Although there may well be a feedback in which the cooling generates an ACC, which then leads to further cooling, and so on. Nevertheless, the generation of a strong ACC can clearly have large consequences for the exchange of heat and carbon between the deep ocean and the atmosphere, and consequently play a crucial role for changes in the global climate system.

Data Availability Statement

Model simulation outputs used in this study is available at Xing (2023).

Acknowledgments

This research was funded by the Australian Research Council Discovery Project (DP180102280). QX was supported by scholarships from the Australian Government Research Training Program (RTP) and CSIRO-UTAS PhD Program in Quantitative Marine Science (QMS). Andreas Klocker is supported by the Research Council of Norway through project KeyPOCP (Studies of Key Polar Ocean and Climate Processes with high resolution coupled climate models). This research was undertaken on the National Computational Infrastructure (NCI) in Canberra, Australia, which is supported by the Australian Commonwealth Government. We are grateful to three anonymous reviewers for their valuable comments that improved the manuscript. We are also grateful to the editor Kris Karnauskas for help and guidance. Open access publishing facilitated by University of Tasmania, as part of the Wiley - University of Tasmania agreement via the Council of Australian University Librarians.

References

Allison, L., Johnson, H., Marshall, D., & Munday, D. (2010). Where do winds drive the Antarctic Circumpolar Current? *Geophysical Research Letters*, *37*(12), L12605. https://doi.org/10.1029/2010gl043355

Baatsen, M., Von Der Heydt, A. S., Huber, M., Kliphuis, M. A., Bijl, P. K., Sluijs, A., & Dijkstra, H. A. (2020). The middle to late Eocene greenhouse climate modelled using the CESM 1.0. 5. *Climate of the Past*, *16*(6), 2573–2597. https://doi.org/10.5194/cp-16-2573-2020

Barkan, R., Winters, K. B., & Smith, S. G. L. (2013). Rotating horizontal convection. *Journal of Fluid Mechanics*, *723*, 556–586. https://doi.org/10.1017/jfm.2013.136

Bernard, B., Madec, G., Penduff, T., Molines, J.-M., Treguier, A.-M., Le Sommer, J., et al. (2006). Impact of partial steps and momentum advection schemes in a global ocean circulation model at eddy-permitting resolution. *Ocean Dynamics*, *56*(5–6), 543–567. https://doi.org/10.1007/s10236-006-0082-1

Delworth, T. L., Rosati, A., Anderson, W., Adcroft, A. J., Balaji, V., Benson, R., et al. (2012). Simulated climate and climate change in the GFDL CM2. 5 high-resolution coupled climate model. *Journal of Climate*, *25*(8), 2755–2781. https://doi.org/10.1175/jcli-d-11-00316.1

Donohue, K., Tracey, K., Watts, D., Chidichimo, M. P., & Chereskin, T. (2016). Mean Antarctic Circumpolar Current transport measured in Drake Passage. *Geophysical Research Letters*, *43*(22), 11–760. https://doi.org/10.1002/2016gl070319

Gayen, B., & Griffiths, R. W. (2022). Rotating horizontal convection. *Annual Review of Fluid Mechanics*, *54*(1), 105–132. https://doi.org/10.1146/annurev-fluid-030121-115729

Gnanadesikan, A. (1999). A simple predictive model for the structure of the oceanic pycnocline. *Science*, *283*(5410), 2077–2079. https://doi.org/10.1126/science.283.5410.2077

Goldner, A., Herold, N., & Huber, M. (2014). Antarctic glaciation caused ocean circulation changes at the Eocene–Oligocene transition. *Nature*, *511*(7511), 574–577. https://doi.org/10.1038/nature13597

Hallberg, R., & Gnanadesikan, A. (2001). An exploration of the role of transient eddies in determining the transport of a zonally reentrant current. *Journal of Physical Oceanography*, *31*(11), 3312–3330. https://doi.org/10.1175/1520-0485(2001)031<3312:aeotro>2.0.co;2

Hallberg, R., & Gnanadesikan, A. (2006). The role of eddies in determining the structure and response of the wind-driven southern hemisphere overturning: Results from the modeling eddies in the southern ocean (MESO) project. *Journal of Physical Oceanography*, *36*(12), 2232–2252. https://doi.org/10.1175/jpo2980.1

Hill, D. J., Haywood, A. M., Valdes, P. J., Francis, J. E., Lunt, D. J., Wade, B. S., & Bowman, V. C. (2013). Paleogeographic controls on the onset of the Antarctic Circumpolar Current. *Geophysical Research Letters*, *40*(19), 5199–5204. https://doi.org/10.1002/grl.50941

Hogg, A. M. (2010). An Antarctic Circumpolar Current driven by surface buoyancy forcing. *Geophysical Research Letters*, *37*(23), L23601. https://doi.org/10.1029/2010gl044777

Hughes, G. O., & Griffiths, R. W. (2008). Horizontal convection. *Annual Review of Fluid Mechanics*, *40*(1), 185–208. https://doi.org/10.1146/annurev.fluid.40.111406.102148

Hutchinson, D. K., de Boer, A. M., Coxall, H. K., Caballero, R., Nilsson, J., & Baatsen, M. (2018). Climate sensitivity and meridional overturning circulation in the late Eocene using GFDL CM2. 1. *Climate of the Past*, *14*(6), 789–810. https://doi.org/10.5194/cp-14-789-2018

Johnson, G. C., & Bryden, H. L. (1989). On the size of the Antarctic Circumpolar Current. Deep Sea Research Part A. *Oceanographic Research Papers*, *36*(1), 39–53. https://doi.org/10.1016/0198-0149(89)90017-4

Johnson, G. C., Schmidtko, S., & Lyman, J. M. (2012). Relative contributions of temperature and salinity to seasonal mixed layer density changes and horizontal density gradients. *Journal of Geophysical Research*, *117*(C4), C04015. https://doi.org/10.1029/2011jc007651

Kiss, A. E., Hogg, A. M., Hannah, N., Boeira Dias, F., Brassington, G. B., Chamberlain, M. A., et al. (2020). ACCESS-OM2 v1. 0: A global ocean–sea ice model at three resolutions. *Geoscientific Model Development*, *13*(2), 401–442. https://doi.org/10.5194/gmd-13-401-2020

Klocker, A., Munday, D., Gayen, B., Roquet, F., & LaCasce, J. H. (2023). Deep-reaching global ocean overturning circulation generated by surface buoyancy forcing. *ESS Open Archive*. https://doi.org/10.22541/essoar.169447446.64699431/v1

Ladant, J.-B., Donnadieu, Y., & Dumas, C. (2014). Links between CO_2, glaciation and water flow: Reconciling the Cenozoic history of the Antarctic Circumpolar Current. *Climate of the Past*, *10*(6), 1957–1966. https://doi.org/10.5194/cp-10-1957-2014

Lefebvre, V., Donnadieu, Y., Sepulchre, P., Swingedouw, D., & Zhang, Z.-S. (2012). Deciphering the role of southern gateways and carbon dioxide on the onset of the Antarctic Circumpolar Current. *Paleoceanography*, *27*(4), PA4201. https://doi.org/10.1029/2012pa002345

Le Traon, P., Nadal, F., & Ducet, N. (1998). An improved mapping method of multisatellite altimeter data. *Journal of Atmospheric and Oceanic Technology*, *15*(2), 522–534. https://doi.org/10.1175/1520-0426(1998)015<0522:aimmom>2.0.co;2

Mak, J., Maddison, J. R., Marshall, D. P., & Munday, D. R. (2018). Implementation of a geometrically informed and energetically constrained mesoscale eddy parameterization in an ocean circulation model. *Journal of Physical Oceanography*, *48*(10), 2363–2382. https://doi.org/10.1175/jpo-d-18-0017.1

Marshall, D. (1997). Subduction of water masses in an eddying ocean. *Journal of Marine Research*, *55*(2), 201–222. https://doi.org/10.1357/0022240973224373

Marshall, J., Adcroft, A., Hill, C., Perelman, L., & Heisey, C. (1997). A finite-volume, incompressible Navier Stokes model for studies of the ocean on parallel computers. *Journal of Geophysical Research*, *102*(C3), 5753–5766. https://doi.org/10.1029/96jc02775

Marshall, J., Hill, C., Perelman, L., & Adcroft, A. (1997). Hydrostatic, quasi-hydrostatic, and nonhydrostatic ocean modeling. *Journal of Geophysical Research*, *102*(C3), 5733–5752. https://doi.org/10.1029/96jc02776

Marshall, J., & Radko, T. (2003). Residual-mean solutions for the Antarctoc Circumpolar Current and its associated overturning circulation. *Journal of Physical Oceanography*, *33*(11), 2341–2354. https://doi.org/10.1175/1520-0485(2003)033<2341:rsftac>2.0.co;2

Mazloff, M. R., Heimbach, P., & Wunsch, C. (2010). An eddy-permitting Southern Ocean state estimate. *Journal of Physical Oceanography*, *40*(5), 880–899. https://doi.org/10.1175/2009jpo4236.1

McDermott, D. (1996). The regulation of northern hemisphere overturning by southern hemisphere winds. *Journal of Physical Oceanography*, *26*(7), 1234–1255. https://doi.org/10.1175/1520-0485(1996)026<1234:tronob>2.0.co;2

Meijers, A. J., Shuckburgh, E., Bruneau, N., Sallée, J.-B., Bracegirdle, T. J., & Wang, Z. (2012). Representation of the Antarctic Circumpolar Current in the CMIP5 climate models and future changes under warming scenarios. *Journal of Geophysical Research*, *117*(C12), C12008. https://doi.org/10.1029/2012jc008412

Meredith, M. P., Woodworth, P. L., Chereskin, T. K., Marshall, D. P., Allison, L. C., Bigg, G. R., et al. (2011). Sustained monitoring of the southern Ocean at Drake Passage: Past achievements and future priorities. *Reviews of Geophysics*, *49*(4), RG4005. https://doi.org/10.1029/2010rg000348

Munday, D. R., Johnson, H. L., & Marshall, D. P. (2013). Eddy saturation of equilibrated circumpolar currents. *Journal of Physical Oceanography*, *43*(3), 507–532. https://doi.org/10.1175/jpo-d-12-095.1

Munday, D. R., Johnson, H. L., & Marshall, D. P. (2015). The role of ocean gateways in the dynamics and sensitivity to wind stress of the early Antarctic Circumpolar Current. *Paleoceanography*, *30*(3), 284–302. https://doi.org/10.1002/2014pa002675

Munday, D. R., Sauermilch, I., Klocker, A., & Whittaker, J. M. (2022). Impact of deep water formation on Antarctic Circumpolar transport during gateway opening. *Authorea Preprints*. https://doi.org/10.22541/essoar.167160849.98375746/v1

Munday, D. R., Zhai, X., Harle, J., Coward, A. C., & Nurser, A. G. (2021). Relative vs. absolute wind stress in a circumpolar model of the Southern Ocean. *Ocean Modelling*, *168*, 101891. https://doi.org/10.1016/j.ocemod.2021.101891

Rintoul, S. R., Hughes, C. W., & Olbers, D. (2001). The Antarctic Circumpolar Current system. In *International geophysics* (Vol. 77, pp. 271–XXXVI). Elsevier.

Rintoul, S. R., & Sokolov, S. (2001). Baroclinic transport variability of the Antarctic Circumpolar Current south of Australia (WOCE repeat section SR3). *Journal of Geophysical Research*, *106*(C2), 2815–2832. https://doi.org/10.1029/2000jc900107

Roquet, F., Ferreira, D., Caneill, R., Schlesinger, D., & Madec, G. (2022). Unique thermal expansion properties of water key to the formation of sea ice on earth. *Science Advances*, *8*(46), eabq0793. https://doi.org/10.1126/sciadv.abq0793

Sauermilch, I., Whittaker, J. M., Klocker, A., Munday, D. R., Hochmuth, K., Bijl, P. K., & LaCasce, J. H. (2021). Gateway-driven weakening of ocean gyres leads to Southern Ocean cooling. *Nature Communications*, *12*(1), 1–8. https://doi.org/10.1038/s41467-021-26658-1

Scher, H. D., Whittaker, J. M., Williams, S. E., Latimer, J. C., Kordesch, W. E., & Delaney, M. L. (2015). Onset of Antarctic Circumpolar Current 30 million years ago as Tasmanian gateway aligned with westerlies. *Nature*, *523*(7562), 580–583. https://doi.org/10.1038/nature14598

Send, U., & Marshall, J. (1995). Integral effects of deep convection. *Journal of Physical Oceanography*, *25*(5), 855–872. https://doi.org/10.1175/1520-0485(1995)025<0855:ieodc>2.0.co;2

Sijp, W. P., & England, M. H. (2004). Effect of the Drake Passage throughflow on global climate. *Journal of Physical Oceanography*, *34*(5), 1254–1266. https://doi.org/10.1175/1520-0485(2004)034<1254:eotdpt>2.0.co;2

Sijp, W. P., England, M. H., & Huber, M. (2011). Effect of the deepening of the Tasman Gateway on the global ocean. *Paleoceanography*, *26*(4). https://doi.org/10.1029/2011pa002143

Sohail, T., Vreugdenhil, C. A., Gayen, B., & Hogg, A. M. (2019). The impact of turbulence and convection on transport in the Southern Ocean. *Journal of Geophysical Research: Oceans*, *124*(6), 4208–4221. https://doi.org/10.1029/2018jc014883

Stickley, C. E., Brinkhuis, H., Schellenberg, S. A., Sluijs, A., Röhl, U., Fuller, M., et al. (2004). Timing and nature of the deepening of the Tasmania gateway. *Paleoceanography*, *19*(4), PA4027. https://doi.org/10.1029/2004pa001022

Straub, D. N. (1993). On the transport and angular momentum balance of channel models of the Antarctic Circumpolar Current. *Journal of Physical Oceanography*, *23*(4), 776–782. https://doi.org/10.1175/1520-0485(1993)023<0776:ottaam>2.0.co;2

Talley, L. D. (1996). Pacific Ocean: Vertical sections and gridded data files for WHP and other selected lines. Retrieved from http://sam.ucsd.edu/vertical_sections/WHP_Pacific_public.html#p16

Tansley, C. E., & Marshall, D. P. (2001). On the dynamics of wind-driven circumpolar currents. *Journal of Physical Oceanography*, *31*(11), 3258–3273. https://doi.org/10.1175/1520-0485(2001)031<3258:otdowd>2.0.co;2

Toggweiler, J., & Samuels, B. (1995). Effect of Drake Passage on the global thermohaline circulation. *Deep-Sea Research*, *42*(4), 477–500. https://doi.org/10.1016/0967-0637(95)00012-u

Toggweiler, J., & Samuels, B. (1998). On the ocean's large-scale circulation near the limit of no vertical mixing. *Journal of Physical Oceanography*, *28*(9), 1832–1852. https://doi.org/10.1175/1520-0485(1998)028<1832:otosls>2.0.co;2

Vallis, G. K. (2017). *Atmospheric and oceanic fluid dynamics: Fundamentals and large-scale circulation* (2nd ed.). Cambridge University Press. https://doi.org/10.1017/9781107588417

Xing, Q. (2023). Deep convection induce strong proto-Antarctic Circumpolar Current [Dataset]. Zenodo. https://doi.org/10.5281/zenodo.7927932

Xing, Q., Klocker, A., Munday, D., & Whittaker, J. (2023). Deepening of southern ocean gateway leads to abrupt onset of a deep-reaching meridional overturning circulation. *Geophysical Research Letters*, *50*(19), e2023GL104382. https://doi.org/10.1029/2023gl104382

Xing, Q., Munday, D., Klocker, A., Sauermilch, I., & Whittaker, J. (2022). The sensitivity of the Eocene–Oligocene Southern Ocean to the strength and position of wind stress. *Climate of the Past*, *18*(12), 2669–2693. https://doi.org/10.5194/cp-18-2669-2022

References From the Supporting Information

Abernathey, R., Marshall, J., & Ferreira, D. (2011). The dependence of Southern Ocean meridional overturning on wind stress. *Journal of Physical Oceanography*, *41*(12), 2261–2278. https://doi.org/10.1175/jpo-d-11-023.1

Dufour, C. O., Sommer, J. L., Gehlen, M., Orr, J. C., Molines, J.-M., Simeon, J., & Barnier, B. (2013). Eddy compensation and controls of the enhanced sea-to-air CO_2 flux during positive phases of the southern annular mode. *Global Biogeochemical Cycles*, *27*(3), 950–961. https://doi.org/10.1002/gbc.20090

Hill, C., Ferreira, D., Campin, J.-M., Marshall, J., Abernathey, R., & Barrier, N. (2012). Controlling spurious diapycnal mixing in eddy-resolving height-coordinate ocean models–insights from virtual deliberate tracer release experiments. *Ocean Modelling*, *45*, 14–26. https://doi.org/10.1016/j.ocemod.2011.12.001

Morrison, A., Saenko, O., Hogg, A. M., & Spence, P. (2013). The role of vertical eddy flux in Southern Ocean heat uptake. *Geophysical Research Letters*, *40*(20), 5445–5450. https://doi.org/10.1002/2013gl057706

Morrison, A. K., Hogg, A. M., & Ward, M. L. (2011). Sensitivity of the southern ocean overturning circulation to surface buoyancy forcing. *Geophysical Research Letters*, *38*(14), L14602. https://doi.org/10.1029/2011gl048031

Munday, D., & Zhai, X. (2015). Sensitivity of southern ocean circulation to wind stress changes: Role of relative wind stress. *Ocean Modelling*, *95*, 15–24. https://doi.org/10.1016/j.ocemod.2015.08.004

Munday, D. R., & Zhai, X. (2017). The impact of atmospheric storminess on the sensitivity of southern ocean circulation to wind stress changes. *Ocean Modelling*, *115*, 14–26. https://doi.org/10.1016/j.ocemod.2017.05.005

Wolfe, C. L., & Cessi, P. (2011). The adiabatic pole-to-pole overturning circulation. *Journal of Physical Oceanography*, *41*(9), 1795–1810. https://doi.org/10.1175/2011jpo4570.1

Zhai, X., & Munday, D. R. (2014). Sensitivity of Southern Ocean overturning to wind stress changes: Role of surface restoring time scales. *Ocean Modelling*, *84*, 12–25. https://doi.org/10.1016/j.ocemod.2014.09.004

Zika, J. D., Le Sommer, J., Dufour, C. O., Naveira-Garabato, A., & Blaker, A. (2013). Acceleration of the Antarctic Circumpolar Current by wind stress along the coast of Antarctica. *Journal of Physical Oceanography*, *43*(12), 2772–2784. https://doi.org/10.1175/jpo-d-13-091.1